SPECT Imaging of Inflammatory Response in Ischemic–Reperfused Rat Hearts Using a ^{99m}Tc-Labeled Dual-Domain Cytokine Ligand

Zhonglin Liu[1], Christy Barber[1], Li Wan[1], Shan Liu[2], Mizhou M. Hui[2,3], Lars R. Furenlid[1], Hua Xu[4], and James M. Woolfenden[1]

[1]Department of Medical Imaging, University of Arizona, Tucson, Arizona; [2]National Key Laboratory of Biochemical Engineering, Institute of Process Engineering, Chinese Academy of Sciences, Beijing, China; [3]AmProtein Corporation, San Gabriel, California; and [4]Department of Pediatrics, University of Arizona, Tucson, Arizona

Soluble tumor necrosis factor (TNF) receptor-2 (TNFR2) and interleukin-1 receptor antagonist (IL-1ra) were fused to the Fc portion of IgG1 using recombinant DNA technology. The resulting dual-domain cytokine ligand, TNFR2-Fc-IL-1ra, specifically binds to TNF and to the type I IL-1 receptor (IL-1RI). This study was designed to characterize the kinetic profile of ^{99m}Tc-labeled TNFR2-Fc-IL-1ra (TFI) for imaging inflammatory response in an ischemic–reperfused (IR) rat heart model. **Methods:** The IR model was created by ligating the left coronary artery for 45 min, followed by 2-h reperfusion. Cardiac SPECT images of TFI in the IR model ($n = 6$) were dynamically acquired for 3 h. Correlative data of myocardial TFI distribution versus microsphere-determined tissue blood flow were acquired in 3 extra IR hearts. Inflammation targeting affinity of TFI was compared with 2 individual cytokine radioligands, ^{99m}Tc-IL-1ra-Fc (IF) and ^{99m}Tc-TNFR2-Fc (TF) ($n = 6$ each group). Myocardial cytokine expression was evaluated by immunochemical assay. **Results:** Increased TFI uptake was found in the ischemic area and correlated with the severity of ischemia. At 3 h after injection, the ratio of hot-spot accumulation in the ischemic area to a remote viable zone was 5.39 ± 1.11 for TFI, which was greater than that for IF (3.28 ± 0.81) and TF (3.29 ± 0.75) ($P < 0.05$). The in vivo uptake profiles of TFI, TF, and IF were consistent with ex vivo radioactive measurements and correlated with upregulated IL-1 and TNF expression. **Conclusion:** The dual-domain TFI is promising for noninvasive detection of inflammatory reactions in IR myocardium because of its more potent affinity to the inflammatory sites compared with TF and IF.

Key Words: interleukin-1; tumor necrosis factor; inflammation; ^{99m}Tc; myocardial ischemia-reperfusion

J Nucl Med 2013; 54:2139–2145
DOI: 10.2967/jnumed.113.123497

Inflammation after myocardial ischemia–reperfusion has been implicated as a crucial factor in expansion of injury (*1–4*). When reperfusion of the ischemic area begins, there is an intense inflammatory reaction that occurs during both the early and the late phases of reperfusion (*1,5*). Proinflammatory cytokines are integral components at the ischemic site and play particularly active roles after myocardial reperfusion (*6,7*). Typically, there is robust upregulation of intramyocardial cytokines in the infarct zone and in the noninfarcted myocardium within the first hours to 1 d after myocardial infarction (*8,9*). If the infarct is large, or if the host inflammatory response is exuberant, there can be either sustained cytokine upregulation or a second wave of cytokine upregulation, corresponding to the chronic postinfarct phase. Remarkably, the second wave can also extend to involve the noninfarcted remote zone, mediating an important remodeling process in the entire myocardium (*4,6*). Consequently, the inflammatory reaction may promote contractile and endothelial dysfunction, regional blood flow decrease, and infarct expansion, all of which may result in heart failure and cardiovascular death.

Interleukin-1 (IL-1) is recognized as a master cytokine of local and systemic inflammation (*10,11*). It is critically associated with myocardial ischemia–reperfusion injury. There are 2 related but distinct IL-1 genes, *IL1A* and *IL1B*, encoding IL-1α and IL-1β, respectively. Each IL-1 binds to the same cell surface receptor, termed IL-1 receptor type I (IL-1RI), which is present on nearly all cells (*10,11*). The action of IL-1 is regulated by the structurally related IL-1 receptor antagonist (IL-1ra), which is primarily produced by activated monocytes and tissue macrophages (*12,13*). IL-1ra is a specific receptor antagonist for IL-1α and IL-1β; it binds to IL-1RI and prevents IL-1 from binding to the same IL-1 receptor (*14*).

Tumor necrosis factor (TNF) is another proinflammatory cytokine that possesses significant inflammatory activity. There are 2 types of TNF, TNF-α and TNF-β, which are mammalian-secreted proteins capable of inducing a wide variety of effects on a large number of cell types. TNF-α is essential in triggering or amplifying local inflammatory responses to ischemia–reperfusion injury (*1*). Cardiac myocytes, mast cells, macrophages, endothelial cells, neutrophils, and monocytes are all possible sources of TNF-α in the ischemic–reperfused (IR) heart (*15,16*). TNF initiates its biologic effects by binding to 2 distinct forms of TNF receptor (TNFR), type I TNFR (TNFR1) and type II TNFR (TNFR2), on the plasma membrane of TNF-responsive cells. The TNF receptors undergo proteolytic cleavage and release a fragment called soluble TNF receptor (soluble TNFR1 or TNFR2), which is a natural antagonist of TNF (*17*).

There are coordinated effects between TNF-α and IL-1β in the inflammatory process associated with myocardial ischemia–reperfusion injury (*18,19*). For example, TNF-α, which alone has no effect on

Received Mar. 21, 2013; revision accepted Aug. 6, 2013.
For correspondence or reprints contact: Zhonglin Liu, University of Arizona, P.O. Box 245067, Tucson, AZ 85724-5067.
E-mail: zliu@radiology.arizona.edu
Published online Oct. 31, 2013.

nitric oxide (NO) production in myocytes, greatly potentiates IL-1β–induced NO production (*20*). TNF-α and IL-1β in cardiac fibroblasts converge on the same pathway to increase the messenger RNA production of angiotensin II type 1 receptor (*21*). The synergistic effects of TNF-α and IL-1β suggest that strategies targeting multiple proinflammatory pathways simultaneously may be more effective than those that target a single pathway. The potential for using the synergistic effects of cytokines motivated us to develop a radiolabeled dual-domain cytokine ligand, ^{99m}Tc-TNFR2-Fc-IL-1ra, for noninvasive imaging assessment of inflammation (*22,23*). TNFR2-Fc-IL-1ra contains a carboxy-terminal segment with the sequence of IL-1ra that specifically binds to cell membrane–bound IL-1RI and an amino-terminal segment that specifically binds to soluble TNF as well as membrane-bound TNF. Using a mouse model with skin inflammation, we have previously demonstrated that ^{99m}Tc-TNFR2-Fc-IL-1ra has more potent affinity to inflammatory sites than the single-domain radioligands ^{99m}Tc-IL-1ra-Fc and ^{99m}Tc-TNFR2-Fc (*22*). In the present study, we hypothesize that uptake of ^{99m}Tc-TNFR2-Fc-IL-1ra in the myocardium is a sensitive indicator of myocardial inflammatory reactions related to acute ischemia–reperfusion injury. This study was designed to investigate the myocardial kinetics of ^{99m}Tc-TNFR2-Fc-IL-1ra for assessing inflammatory response in an IR rat heart model. We compared the inflammation targeting affinity of ^{99m}Tc-TNFR2-Fc-IL-1ra with that of ^{99m}Tc-TNFR2-Fc and ^{99m}Tc-IL-1ra-Fc.

MATERIALS AND METHODS

Radiolabeling

Recombinant TNFR2-Fc-IL-1ra and IL-1ra-Fc were produced at AmProtein Corp. as previously described (*22,23*). TNFR2-Fc (anakinra, Kineret) was purchased from Amgen Inc. The ligands were ^{99m}Tc-labeled using a modified direct protocol (*24,25*) in which glucoheptonic acid serves as a transfer agent to chelate tin-reduced $^{99m}TcO_4^-$ to thiolated proteins by 2-iminothiolane (2-IT) at a 2-IT/protein ratio of 1,000. Radiolabeling efficiency (radiochemical purity) determined by size-exclusion high-performance liquid chromatography was always greater than 97% in gel-purified products.

IR Rat Heart Model

Male Sprague–Dawley rats (250–300 g) were anesthetized with 1.0%–1.5% isoflurane and ventilated using an Inspira Advanced Safety Ventilator (Harvard Apparatus) with a mixture of oxygen and room air. The chest was opened at the fourth or fifth intercostal space. Using a curved and tapered needle with a 6.0 Prolene suture (Ethicon), we placed a ligature around the left coronary artery (LCA) and pulled tight by passing the suture through a polyethylene tubing and clamping it for a 45-min occlusion. Myocardial reperfusion was achieved by releasing the ligature 120 min before a radiotracer was intravenously injected. The chest of the rat was closed for SPECT imaging.

SPECT Imaging of IR Hearts with Cytokine Radioligands

A small-animal stationary SPECT imager called FastSPECT II was used to image the IR rat hearts. FastSPECT II is capable of acquiring projection data without any motion of the object or detection system. The spatial resolution is about 1 mm, with a 16-pinhole aperture.

Six anesthetized rats with myocardial IR treatments were dynamically imaged for 3 h to determine the ^{99m}Tc-TNFR2-Fc-IL-1ra cardiac kinetic profile. ^{99m}Tc-TNFR2-Fc-IL-1ra (111–166.5 MBq [3.0–4.5 mCi], 0.3 mL) was intravenously injected via a preinstalled tail vein catheter using a PHD2000 syringe pump (Harvard Apparatus). Immediately after injection, cardiac images were acquired every minute for 10 min, followed by 5-min acquisitions at 15, 20, 30, 45, 60, 120, and 180 min after injection to generate 16 projection datasets for tomographic reconstructions.

The rat IR heart model was also used to compare ^{99m}Tc-TNFR2-Fc-IL-1ra targeting affinity with that of ^{99m}Tc-IL-1ra-Fc and ^{99m}Tc-TNFR2-Fc. The rats in each group (n = 6) received 1 of the cytokine radioligands (111–166.5 MBq [3.0–4.5 mCi], 0.3 mL) via tail vein injection. The rats were allowed to recover and have free access to food and water for 3 h. The rats were subsequently imaged for 10 min using FastSPECT II and then sacrificed for postmortem analysis.

SPECT Image Processing

Tomographic reconstructions of FastSPECT II data were processed using 25 iterations of the ordered-subset expectation maximization algorithm and computed to provide 3-dimensional images in an 81 × 121 × 121 voxel format with AMIDE 0.9.1 software to generate transverse, coronal, and sagittal slices with 1-voxel thickness (1.0 mm).

Dynamic analysis of myocardial activity in the IR hearts was performed with computerized 3-dimensional region-of-interest analysis. The regions of interest were first established over normal myocardial zones and ischemic areas with high radioactive uptake (hot spot) on the 180-min images for determining average counts per pixel. The regions of interest on the 180-min images were applied to all of the dynamic images for determining average counts per pixel from 1 to 180 min after injection. After correction for acquisition time and decay, time–activity curves over the normal zones and infarct areas were plotted by normalizing radioactive counts at each time point to peak uptake counts. This normalization was used to eliminate the variation of injected doses.

Postmortem Analysis of IR Rat Hearts

After imaging, the LCA was reoccluded. Evans blue (20%) in 1.0 mL of phosphate-buffered saline buffer was injected through the femoral vein, allowing dye to stain the nonischemic portion of the heart. An overdose injection of Beuthanasia-D (100 mg/kg; Schering-Plough Animal Health Corp.) was administered immediately thereafter to sacrifice the animal. The entire heart was expeditiously excised, weighed, and rinsed of excess dye with cold saline. ^{99m}Tc activity in the heart was measured in a CRC-15W radioisotope dose calibrator (Capintec). The left ventricle was sectioned into 1-mm slices in a plane parallel to the atrioventricular groove. Both sides of each tissue slice were photographed for measuring the ischemic area at risk (IAR).

In the rats with dynamic ^{99m}Tc-TNFR2-Fc-IL-1ra imaging, the left ventricular slices were incubated in 1% triphenyltetrazolium chloride (TTC) PBS-buffered solution (pH 7.4) at 37C° for 20 min and subsequently fixed in 10% PBS-buffered formalin overnight at 2°C–8°C. Both sides of each TTC-stained tissue slice were photographed again. The viable myocardium stained by TTC appeared dark red, and necrotic myocardium appeared white or pale.

^{99m}Tc-TNFR2-Fc-IL-1ra Distribution Versus Myocardial Blood Flow (MBF)

Stable, nonradioactive isotope–labeled microspheres provided by BioPAL, Inc. were used to determine the regional blood flow in rat hearts by neutron-activation analysis (*26,27*). The correlation between myocardial ^{99m}Tc-TNFR2-Fc-IL-1ra distribution and regional MBF was determined in 3 additional IR rat hearts. Briefly, a carotid artery was catheterized to provide a site for microsphere reference blood withdrawal. Ten minutes after LCA ligation when the heart beating was stable, a set of 15-μm-diameter Gold STER/spheres microspheres (2.5×10^6) diluted in 1.0 mL of sansSaline obtained from BioPAL was directly injected into the left ventricle for 10 s. A reference blood sample (1.8 mL) was withdrawn from the carotid artery by the Harvard infusion/withdrawal syringe pump beginning 10 s before injection of microspheres and continuing for 70 s at a constant rate of 1.5 mL/min. An equal amount of blood from a donor rat was given after the reference blood sample was collected. Two hours after reperfusion, ^{99m}Tc-TNFR2-Fc-IL-1ra was injected through a jugular vein catheter. Three hours later (5 h after reperfusion), 15-μm-diameter Samarium STER/spheres

microspheres (2.5×10^6) diluted in 1.0 mL of sansSaline were injected into the left ventricle, followed by blood-sample collection as described above. The heart was excised, and the left ventricle was divided into 0.05- to 0.1-g pieces to measure ^{99m}Tc radioactivity. The blood samples were prepared according to the vendor's instructions. All samples were shipped to BioPAL for neutron-activation analysis and quantification.

Western Blot Analysis of IL-1β, IL-1RI, and TNF-α

Two randomly selected IR rat hearts from each group were harvested. The left ventricle was separated into nonischemic healthy myocardium and IAR determined by Evans blue staining. The samples were processed using a snap freezing procedure by which samples were lowered to temperatures below −70°C rapidly with liquid nitrogen and stored in a −80°C freezer until use. The frozen samples were homogenized in radioimmunoprecipitation assay (RIPA) buffer containing 1 mM phenylmethylsulfonyl fluoride and 1X Halt protease and phosphatase inhibitor cocktail (Thermo Scientific) using a tissue homogenizer. The tissue homogenates were centrifuged at 10,000*g* at 4°C for 10 min. The supernatants were collected and centrifuged again at 10,000*g* at 4°C for 10 min. Protein concentration in the supernatant was determined using a Pierce BCA Protein Assay kit (Thermo Scientific). Tissue lysate (40 μg of protein) was separated on polyacrylamide gel electrophoresis (PAGE) gel and then transferred to a nitrocellulose membrane. Rabbit polyclonal antibodies were purchased from Santa Cruz Biotechnology, Inc., for detection of IL-1β, IL-1RI, and TNF-α. Goat antirabbit IgG antibody, used as a secondary antibody, was also purchased from Santa Cruz Biotechnology, Inc.

Detection of IL-1β and TNF-α by Enzyme-Linked Immunosorbent Assays (ELISA)

Snap frozen IAR and nonischemic myocardial tissues were homogenized in a cell-extraction buffer (Invitrogen Corp.) containing 10 mM Tris (pH 7.4), 100 mM NaCl, 1 mM ethylenediaminetetraacetic acid (EDTA), 1 mM ethylene glycol tetraacetic acid (EGTA), 1 mM NaF, 20 mM $Na_4P_2O_7$, 2 mM Na_3VO_4, 1% Triton X-100, 10% glycerol, 0.1% sodium dodecyl sulfate (SDS), and 0.5% deoxycholate. Immediately before the tissue was processed, 1 mM phenylmethylsulfonyl fluoride and protease inhibitor cocktail (Sigma-Aldrich Corp.) was added into the cell-extraction buffer. The final homogenate was centrifuged at 20,000*g* at 4°C for 15 min. Protein concentration was determined using the BCA Protein Assay Kit. The supernatant fraction was aliquoted and frozen at −80°C until solid-phase sandwich ELISA was performed for determination of cytokine protein levels.

The levels of myocardial IL-1β and TNF-α were determined in 8 IR rat hearts using ELISA kits purchased from Invitrogen Corp. Briefly, diluted samples and standards at 100 μL (IL-1) were transferred to the antibody-coated wells in a 96-well polyvinyl plate. The plates were incubated for 90 min at room temperature, and the wells were washed with wash solution. A solution of enzyme-conjugated detection antibody was added. After a second incubation for 30 min and washing, a substrate solution containing tetramethylbenzidine/H_2O_2 was added. After 30-min incubation, the stop solution (0.5 Mol/L H_2SO_4) was added and the plates were read using a DTX 880 Multimode Detector (Beckman Coulter, Inc.) at a wavelength of 450 nm. The results of IL-1β and TNFα measurements were expressed as pg/mL and corrected for total protein (pg/mg).

Data Analysis

All quantitative results were expressed as mean ± SEM. Comparisons between 2 variables were performed with 1-way ANOVA. Probability values of less than 0.05 were considered significant.

Ethics

The animal experiments were performed in accordance with *Guide for the Care and Use of Laboratory Animals* (*28*) and were approved by the Institutional Animal Care and Use Committee at the University of Arizona.

RESULTS

Dynamic Imaging of ^{99m}Tc-TNFR2-Fc-IL-1ra

The in vivo uptake profiles of ^{99m}Tc-TNFR2-Fc-IL-1ra in the IR hearts were depicted in dynamic tomographic images. Blood-pool activity was seen immediately after injection, with gradual washout starting around 10 min. Focal radioactive accumulation (hot spot) in the anterior and lateral walls of the left ventricle became visible by 60–75 min after injection and remained persistent over the 3-h postinjection period. A considerable amount of radioactivity was observed in the liver. Representative dynamic images of ^{99m}Tc-TNFR2-Fc-IL-1ra in an IR heart are shown in Figure 1.

Representative myocardial time–activity curves of ^{99m}Tc-TNFR2-Fc-IL-1ra in ischemic and remote healthy myocardium are summarized in Figure 2. After reaching an initial peak at about 2 min, ^{99m}Tc-TNFR2-Fc-IL-1ra in the healthy myocardium exhibited relatively rapid clearance over the observation period of 180 min after injection. In contrast, ^{99m}Tc-TNFR2-Fc-IL-1ra in the ischemic area showed increasing uptake until 10 min, after which there was slow washout. The kinetic curves plotted from 10 to 180 min showed a significant difference between the remote viable zone and ischemic area with hot-spot accumulation ($P < 0.05$). At 180 min after injection, the myocardial radioactive retention (% peak) was 50.7% ± 8.4% in ischemic myocardium and 14.2% ± 5.5% in remote nonischemic area ($P < 0.01$).

Comparing Targeting Affinity of ^{99m}Tc-TNFR2-Fc-IL-1ra with ^{99m}Tc-TNFR2-Fc and ^{99m}Tc-IL-1ra-Fc

High radioactive accumulations (hot spots) were observed in the myocardial IAR on FastSPECT II images acquired using all three ^{99m}Tc-labeled cytokine ligands. Representative reconstructed images are shown in Figure 3. High radioactive uptake in the liver was observed. The most prominent radioactive uptake in the chest

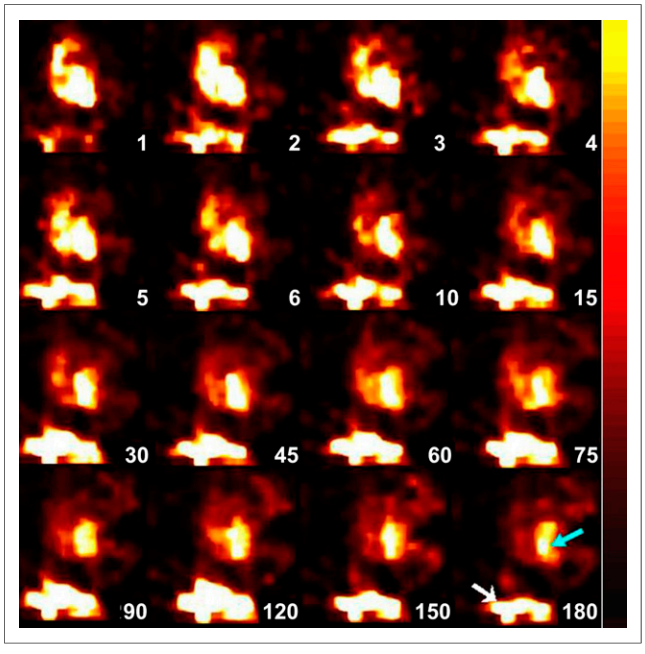

FIGURE 1. Representative dynamic images of ^{99m}Tc-TNFR2-Fc-IL-1ra in an IR rat heart. Coronal slices are at intervals from 1 to 180 min after injection, as indicated by number in each frame. Progressive focal accumulation of radioactivity is demonstrated in myocardial ischemic area (blue arrow on 180-min image). Prominent radioactivity is observed in liver (white arrow).

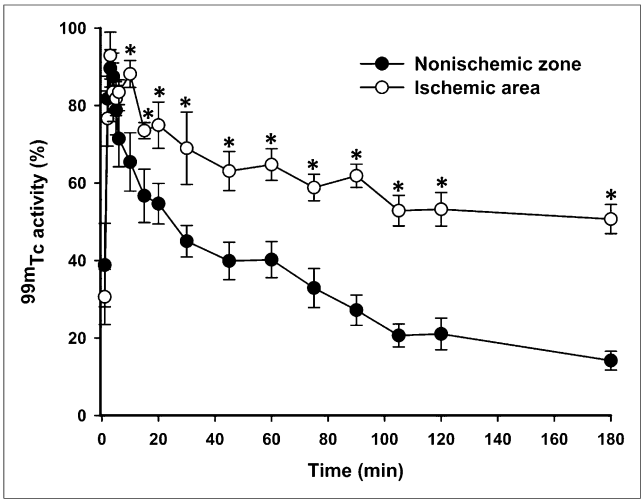

FIGURE 2. Normalized time–activity curves of ^{99m}Tc-TNFR2-Fc-IL-1ra from ischemic area and remote viable zone in rat hearts with ischemia–reperfusion injury. Activity at each time point is normalized to peak activity in each animal. *$P < 0.05$, compared with viable zone.

was found in the anterior wall, lateral wall, and apex of the left ventricle. The dual-domain ^{99m}Tc-TNFR2-Fc-IL-1ra exhibited more potent affinity, with enhanced uptake in the inflammatory sites of IR hearts, than the single-domain ligands. At 3 h after injection, the radioactive ratio of ischemic area to viable zone was 5.42 ± 1.10 for ^{99m}Tc-TNFR2-Fc-IL-1ra, which was greater than ratios for ^{99m}Tc-IL-1ra-Fc (3.28 ± 0.81) and ^{99m}Tc-TNFR2-Fc (3.29 ± 0.75) ($P < 0.05$).

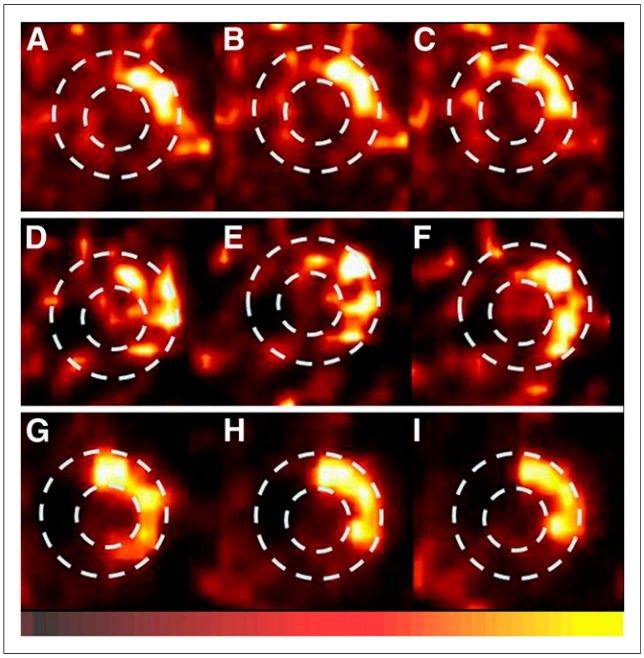

FIGURE 3. Imaging comparison of ^{99m}Tc-IL-1ra-Fc (A–C), ^{99m}Tc-TNFR2-Fc (D–F), and ^{99m}Tc-TNFR2-Fc-IL-1ra (G–I) in rat hearts with 45-min ischemia and 120-min reperfusion. Three representative transaxial slices obtained at 3 h after injection using each radiotracer show radioactive accumulations (hot spots) in ischemic area. Dashed circle indicates margins of left ventricle.

Ex Vivo Measurements of Myocardial Radioactive Uptake

The spatial distributions of ^{99m}Tc-TNFR2-Fc-IL-1ra, ^{99m}Tc-IL-1ra-Fc, and ^{99m}Tc-TNFR2-Fc in left ventricular myocardium were identified by ex vivo radioactive measurement. Myocardial radioactivity levels (percentage injected dose per gram [%ID/g]) in the whole heart, IAR, and nonischemic or remote viable myocardium (positive Evans blue staining) are shown in Table 1. The uptake level of ^{99m}Tc-TNFR2-Fc-IL-1ra in the IAR was significantly greater than that of ^{99m}Tc-TNFR2-Fc and ^{99m}Tc-IL-1ra-Fc. There was no difference between the myocardial uptake of ^{99m}Tc-TNFR2-Fc and ^{99m}Tc-IL-1ra-Fc.

Figure 4 shows representative autoradiographs of ^{99m}Tc-TNFR2-Fc-IL-1ra in IR left ventricular myocardium and photographs of the corresponding myocardial slices stained with Evans blue and TTC. The area of radioactive uptake was comparable in size with the IAR (unstained by Evans blue) and larger than the myocardial infarct size (TTC-negative area).

Correlation Between ^{99m}Tc-TNFR2-Fc-IL-1ra Uptake and MBF

Figure 5 demonstrates the microsphere-determined MBF at LCA occlusion and reperfusion versus ^{99m}Tc-TNFR2-Fc-IL-1ra myocardial uptake. ^{99m}Tc-TNFR2-Fc-IL-1ra uptake was spatially related to the extent of ischemic myocardium and localized primarily in the area surrounding the myocardial necrotic core. When the LCA was occluded, the average MBF for the entire left ventricle was 1.15 ± 0.13 mL/min/g. When coronary flow was restored, the average MBF increased slightly to 1.44 ± 0.09 mL/min/g, but the increase did not reach statistical significance. However, 18 of 31 myocardial samples (from 3 rats) showed less than 1.0 mL/min/g MBF (0.46 ± 0.08) during LCA occlusion. ^{99m}Tc-TNFR2-Fc-IL-1ra uptake (%ID/g) was significantly higher in these myocardial samples than in samples with MBF greater than 1.0 mL/min/g (0.96 ± 0.15 vs. 0.38 ± 0.04, $P < 0.001$). For analysis, we considered tissue samples with an MBF greater than 1.0 mL/min/g as nonischemic myocardium. Samples with an MBF less than 1 mL/min/g during LCA occlusion showed a significant linear correlation with negative slope, −0.25, between ^{99m}Tc-TNFR2-Fc-IL-1ra uptake and MBF ($\gamma = 0.647$, $P = 0.017$). In contrast, tissue samples with MBF greater than or equal to 1.0 mL/min/g showed a nonsignificant linear correlation ($\gamma = 0.271$, $P = 0.277$). AT LCA reflow, ^{99m}Tc-TNFR2-Fc-IL-1ra uptake versus MBF demonstrated a linear correlation with negative slope (slope = −0.378, $\gamma = 0.406$, $P = 0.023$). In this measurement, 6 samples with MBF less than 1.0 mL/min/g (0.66 ± 0.05) had correspondingly higher ^{99m}Tc-TNFR2-Fc-IL-1ra uptake (%ID/g) than tissue pieces with MBF greater than 1.0 mL/min/g (1.10 ± 0.28 vs. 0.51 ± 0.06, $P = 0.003$).

IL-1β and TNF-α Expression in IR Myocardium

Postmortem analysis of lysates prepared from the rat myocardium showed that expression of IL-1 β and TNF-α in the IAR was significantly increased after ischemia–reperfusion. Immunoblot analyses using polyclonal antibodies are illustrated in Figure 6. Antibodies reacted strongly to IL-1β precursor and IL-1RI at the molecular weights of 31 and 80 kDa, respectively. The protein extracts reacted with the anti–TNF-α antibody at an apparent molecular weight of 26 kDa, which is consistent with membrane-bound TNF-α. In the remote control myocardium, IL-1β, IL-1RI, and TNF-α were barely detectable.

After normalization for total protein, ELISA results of cytokine measurements in homogenized myocardial tissue indicated that

TABLE 1
Cardiac Biodistribution (%ID/g) at 3 Hours After Injection

Radioligand	Whole heart	IAR	Remote area
^{99m}Tc-IL-1ra-Fc	0.27 ± 0.03	0.61 ± 0.11*	0.16 ± 0.04
^{99m}Tc-TNFR2-Fc	0.35 ± 0.12	0.81 ± 0.06*	0.24 ± 0.09
^{99m}Tc-TNFR2-Fc-IL-1ra	0.51 ± 0.06†	1.14 ± 0.05*†‡	0.18 ± 0.02

*$P < 0.05$, compared with remote area.
†$P < 0.05$, compared with ^{99m}Tc-IL-1ra-Fc.
‡$P < 0.05$, compared with ^{99m}Tc-TNFR2-Fc.

the expression levels (pg/mg) of IL-1β and TNF-α were significantly increased in IR myocardium, compared with remote control (IL-1β: 1,279.2 ± 144.7 vs. 916.1 ± 46.5, $P = 0.016$; TNF-α: 457.7 ± 30.3 vs. 369.2 ± 20.3, $P = 0.041$).

DISCUSSION

Conventional cardiovascular imaging technologies rely on anatomic, physiologic, or metabolic differences to provide image contrast between normal and inflamed tissue; detection of the inflammatory response is typically indirect or nonspecific. Scintigraphic imaging with radiolabeled leukocytes is a standard clinical procedure for detection of occult infection and inflammation. However, in vitro radiolabeling of leukocytes requires a complicated procedure associated with a potential risk for infection. Radiopharmaceuticals targeting leukocyte receptors hold promise for noninvasive detection of infection and inflammation (*29,30*). However, they provide little insight into the proinflammatory cytokine pathway. ^{18}F-FDG is a sensitive tracer for imaging of inflammation. In subacutely infarcted myocardium, ^{18}F-FDG was found to accumulate relative to the tissue's monocyte or macrophage content (*31*). However, ^{18}F-FDG uptake in normal myocytes poses problems for use of ^{18}F-FDG in detecting inflammation in the heart.

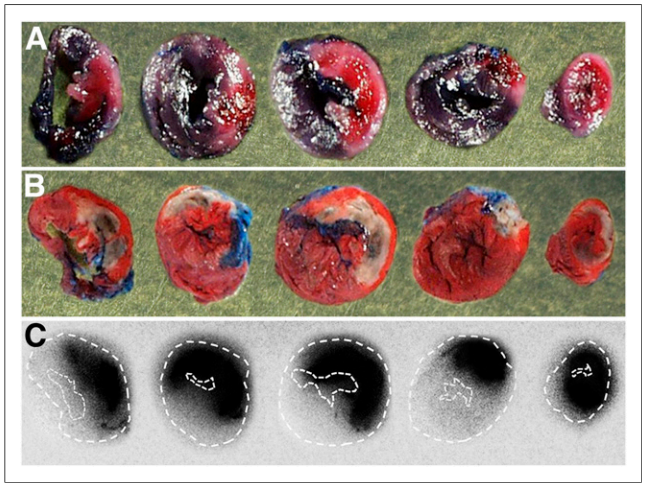

FIGURE 4. Representative photographs of transaxial slices of IR rat heart. (A) IAR (unstained areas) by Evans blue staining. (B) Myocardial infarcts (unstained areas) by TTC staining. (C) ^{99m}Tc-TNFR2-Fc-IL-1ra uptake (dark black areas) by autoradiography. White dashed lines on autoradiographs indicate outlines of left ventricular slices with TTC staining. Distributions of ^{99m}Tc-TNFR2-Fc-IL-1ra were matched to IAR in size but were larger than infarcts on TTC staining.

Radiolabeled cytokines and cytokine ligands are an emerging class of radiopharmaceuticals to detect inflammatory disorders and promote timely therapeutic intervention. Hybrid TNFR1-Fc/TNFR2-Fc has many advantages, compared with natural TNFR1/TNFR2, including specificity, low immunogenicity, and high affinity. As a recombinant cytokine ligand, radiolabeled TNFR2-Fc or TNFR1-Fc usually remains in the bloodstream and binds to blood cells and has limited tissue distribution. Detection of inflammation through the IL-1 pathway would provide important information regarding the underlying pathobiology of many inflammatory and autoimmune diseases. Radiolabeled IL-1ra using structurally modified or unmodified IL-1ra represents an important probe for inflammation imaging (*32,33*). However, radiolabeled IL-1ra showed relatively poor in vivo sensitivity in animal studies, probably because of competition with IL-1 for the IL-1 receptor (*32,33*).

The potential synergetic mechanism between IL-1 and TNF pathways may provide TNFR2-Fc-IL-1ra with an inflammatory targeting effect greater than that of the 2 probes alone or administered concurrently. IL-1ra may extend the biologic half-life of TNFR2-Fc-IL-1ra and direct the dual-domain ligand to IL-1 receptor–rich inflammatory sites (*23*). We have previously shown that in healthy rats, the blood half-life of ^{99m}Tc-TNFR2-Fc-IL-1ra was 140.8 min (*22*). In the same study, we demonstrated that ^{99m}Tc-TNFR2-Fc-IL-1ra was capable of specifically targeting inflammatory sites, as indicated by blocking experiments with unlabeled ligand using an ear inflammation model. More importantly, ^{99m}Tc-TNFR2-Fc-IL-1ra showed greater affinity to the inflamed ear than ^{99m}Tc-IL-1ra-Fc or ^{99m}Tc-TNFR2-Fc. In the present study, ^{99m}Tc-TNFR2-Fc-IL-1ra uptake in IR myocardium was identified by in vivo SPECT and ex vivo autoradiography. The hot-spot uptake of ^{99m}Tc-TNFR2-Fc-IL-1ra corresponded to IAR as determined by postmortem staining with Evans blue, and the involved area was much larger than the myocardial infarct shown by TTC staining. Furthermore, we found that ^{99m}Tc-TNFR2-Fc-IL-1ra had greater uptake in myocardial IR sites than ^{99m}Tc-IL-1ra-Fc or ^{99m}Tc-TNFR2-Fc.

The ischemia–reperfusion procedure resulted in significant inflammatory reactions with upregulated cytokine expression in the present study. First, a local increase in the tissue level of IL-1β was demonstrated by Western blot and ELISA. It has been reported that increased levels of IL-1β could occur for more than several weeks in IR rat heart models (*8,34,35*). The IL-1β pathway plays a major role in mediating transcription of adhesion molecules, chemokines, secondary cytokines, nitric oxide synthase, and cyclooxygenase, all relevant to inflammation reactions. IL-1β is found in macrophages, endothelial cells, and vascular smooth muscle cells in addition to myocytes. Moreover, our Western blot analysis showed

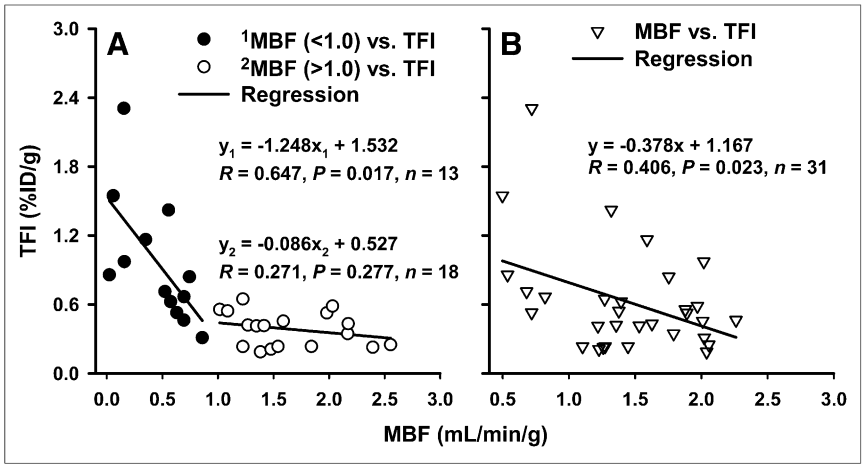

FIGURE 5. Regression analysis of ^{99m}Tc-TNFR2-Fc-IL-1ra (TFI) distribution (%ID/g) versus microsphere-determined MBF in 31 left ventricular myocardial samples from 3 IR rat hearts. MBF (mL/min/g) was measured 10 min after LCA occlusion (A) and 5 h after LCA reflow (B). TFI was intravenously administered at 2 h after LCA reflow. Tissues with blood flow less than 1.0 mL/min/g exhibited significant correlation ($P < 0.05$) with TFI uptake at LCA occlusion and also at LCA reflow.

significantly upregulated local expression of IL-1RI. Second, there was an increase in TNF-α at the IR site. The involvement of TNF-α has been investigated in prior studies with myocardial ischemia–reperfusion injury, with varying results (*9,36–38*). TNF-α was found to increase significantly at 4 h and return to baseline after 8–24 h of reperfusion (*9,36*). In the present study, both Western blotting and ELISA showed significantly upregulated TNF-α expression in IAR at 5 h after reperfusion, though the time of peak TNF-α expression was not determined.

It is not yet clear which cytokine pathway contributed more significantly to the increased uptake of ^{99m}Tc-TNFR2-Fc-IL-1ra. On the basis of the levels of IL-1β and TNF-α expression, both IL-1β and TNF-α pathways might play significant roles. Unlike the IL-1ra domain, which targets IL-1RI competitively with IL-1β, the TNFR2 domain of TNFR2-Fc-IL-1ra can bind to a bioactive membrane-bound form (mTNF) or precursor on TNF-producing cells and the soluble form (sTNF) in the extracellular environment (*39,40*). In principle, sTNF and mTNF are biologic targets for ^{99m}Tc-TNFR2-Fc and the TNFR2-domain of ^{99m}Tc-TNFR2-Fc-IL-1ra. When the TNFR2 domain binds to sTNF or mTNF, the IL-1ra domain can bind to IL-1RI on another cell membrane. The competitive mechanism between natural IL-1β and the IL-1ra domain might diminish ^{99m}Tc-TNFR2-Fc-IL-1ra uptake in the case of a limited number of IL-1RI sites available and overexpression of IL-1β. However, the results of our Western blot analysis indicated that IL-1RI was upregulated more significantly than IL-1β by about 15-fold, and IL-1RI was correlated with the high uptake of ^{99m}Tc-TNFR2-Fc-IL-1ra.

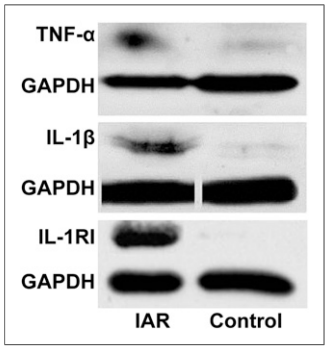

FIGURE 6. Representative Western blot analysis of TNF-α, IL-1β, and transmembrane IL-1RI in homogenized IAR and control myocardium. Glyceraldehyde 3-phosphate dehydrogenase (GAPDH) is shown as protein loading control.

Reestablishing blood flow to ischemic myocardium might promote nonspecific accumulation of radiolabeled molecules because of regional hyperperfusion and microvascular dysfunction induced by ischemia–reperfusion injury. As a result, the radioactivity detected in the ischemic lesions in this study might be a combination of specific cytokine binding and nonspecific distribution of the cytokine radioligands. The contribution of myocardial nonspecific binding and microvascular dysfunctional leakage in the IR rat hearts needs to be quantitatively clarified in further blocking studies using unradiolabeled cold ligands and leakage studies using radiolabeled nonspecific proteins of similar molecular weight. The microsphere perfusion measurements in the present study showed that increasing the severity of ischemia led to enhanced ^{99m}Tc-TNFR2-Fc-IL-1ra uptake in a direct negative linear relationship. ^{99m}Tc-TNFR2-Fc-IL-1ra uptake was markedly increased at a flow less than 0.1 mL/min/g when LCA was occluded. Similar negative linear correlation was found at 5 h after reperfusion. The increase of ^{99m}Tc-TNFR2-Fc-IL-1ra uptake was mostly found in reperfused tissues with blood flow around 0.5 mL/min/g but not in the high blood-flow areas. Thus, the contribution of hyperperfusion effects and vascular leakage issues might not be significant in the myocardial distribution of ^{99m}Tc-TNFR2-Fc-IL-1ra in our model.

CONCLUSION

Inflammatory reactions corresponding to myocardial ischemia–reperfusion injury can be assessed by SPECT imaging using ^{99m}Tc-labeled IL-1ra-Fc, TNFR2-Fc, and TNFR2-Fc-IL-1ra. The dual-domain ^{99m}Tc-TNFR2-Fc-IL-1ra showed more potent affinity, with enhanced uptake in the inflammatory sites of IR hearts, than the single-domain ligands. ^{99m}Tc-TNFR2-Fc-IL-1ra SPECT imaging may provide an effective tool for targeting inflammatory components relating to myocardial ischemia–reperfusion injury. The synergy between TNFR2 and IL-1ra may lead to an inflammatory targeting effect greater than that of either of the 2 probes alone or administered concurrently. Molecular imaging using ^{99m}Tc-TNFR2-Fc-IL-1ra holds promise for specific detection of inflammation via IL-1 and TNF pathways in other inflammatory diseases.

DISCLOSURE

The costs of publication of this article were defrayed in part by the payment of page charges. Therefore, and solely to indicate this fact, this article is hereby marked "advertisement" in accordance with 18 USC section 1734. This work was supported by NIH grants NHLBI R01-HL090716 and NIBIB P41-EB002035. No other potential conflict of interest relevant to this article was reported.

ACKNOWLEDGMENTS

We are grateful to Dr. Gail Stevenson for support in animal studies and protocol development. We thank Dr. Paul McDonagh for allowing use of his laboratory materials and equipment in tissue processing. Dr. Mizhou Hui is an employee and Chief Scientific Officer of AmProtein Corporation.

REFERENCES

1. Blancke F, Claeys MJ, Jorens P, et al. Systemic inflammation and reperfusion injury in patients with acute myocardial infarction. *Mediators Inflamm.* 2005;2005:385–389.
2. Frangogiannis NG. Targeting the inflammatory response in healing myocardial infarcts. *Curr Med Chem.* 2006;13:1877–1893.
3. Jefferson BK, Topol EJ. Molecular mechanisms of myocardial infarction. *Curr Probl Cardiol.* 2005;30:333–374.
4. Ren G, Dewald O, Frangogiannis NG. Inflammatory mechanisms in myocardial infarction. *Curr Drug Targets Inflamm Allergy.* 2003;2:242–256.
5. Zhao ZQ, Velez DA, Wang NP, et al. Progressively developed myocardial apoptotic cell death during late phase of reperfusion. *Apoptosis.* 2001;6: 279–290.
6. Nian M, Lee P, Khaper N, Liu P. Inflammatory cytokines and postmyocardial infarction remodeling. *Circ Res.* 2004;94:1543–1553.
7. Pudil R, Pidrman V, Krejsek J, et al. Cytokines and adhesion molecules in the course of acute myocardial infarction. *Clin Chim Acta.* 1999;280:127–134.
8. Deten A, Volz HC, Briest W, Zimmer HG. Cardiac cytokine expression is upregulated in the acute phase after myocardial infarction. Experimental studies in rats. *Cardiovasc Res.* 2002;55:329–340.
9. Herskowitz A, Choi S, Ansari AA, Wesselingh S. Cytokine mRNA expression in postischemic/reperfused myocardium. *Am J Pathol.* 1995;146:419–428.
10. Dunne A. Inflammasome activation: from inflammatory disease to infection. *Biochem Soc Trans.* 2011;39:669–673.
11. Mills KH, Dunne A. Immune modulation: IL-1, master mediator or initiator of inflammation. *Nat Med.* 2009;15:1363–1364.
12. Eisenberg SP, Evans RJ, Arend WP, et al. Primary structure and functional expression from complementary DNA of a human interleukin-1 receptor antagonist. *Nature.* 1990;343:341–346.
13. Bresnihan B. The prospect of treating rheumatoid arthritis with recombinant human interleukin-1 receptor antagonist. *BioDrugs.* 2001;15:87–97.
14. Efthimiou P, Markenson JA. Role of biological agents in immune-mediated inflammatory diseases. *South Med J.* 2005;98:192–204.
15. Frangogiannis NG, Lindsey ML, Michael LH, et al. Resident cardiac mast cells degranulate and release preformed TNF-alpha, initiating the cytokine cascade in experimental canine myocardial ischemia/reperfusion. *Circulation.* 1998;98: 699–710.
16. Reil JC, Gilles S, Zahler S, et al. Insights from knock-out models concerning postischemic release of TNFα from isolated mouse hearts. *J Mol Cell Cardiol.* 2007;42:133–141.
17. Van Zee KJ, Kohno T, Fischer E, Rock CS, Moldawer LL, Lowry SF. Tumor necrosis factor soluble receptors circulate during experimental and clinical inflammation and can protect against excessive tumor necrosis factor alpha in vitro and in vivo. *Proc Natl Acad Sci USA.* 1992;89:4845–4849.
18. Cain BS, Meldrum DR, Dinarello CA, et al. Tumor necrosis factor-alpha and interleukin-1beta synergistically depress human myocardial function. *Crit Care Med.* 1999;27:1309–1318.
19. Woldbaek PR, Tonnessen T, Henriksen UL, et al. Increased cardiac IL-18 mRNA, pro-IL-18 and plasma IL-18 after myocardial infarction in the mouse; a potential role in cardiac dysfunction. *Cardiovasc Res.* 2003;59:122–131.
20. Kan H, Xie Z, Finkel MS. TNF-alpha enhances cardiac myocyte NO production through MAP kinase-mediated NF-kappaB activation. *Am J Physiol.* 1999;277: H1641–H1646.
21. Gurantz D, Cowling RT, Varki N, Frikovsky E, Moore CD, Greenberg BH. IL-1beta and TNF-alpha upregulate angiotensin II type 1 (AT1) receptors on cardiac fibroblasts and are associated with increased AT1 density in the post-MI heart. *J Mol Cell Cardiol.* 2005;38:505–515.
22. Liu Z, Wyffels L, Barber C, et al. Characterization of ^{99m}Tc-labeled cytokine ligands for inflammation imaging via TNF and IL-1 pathways. *Nucl Med Biol.* 2012;39:905–915.
23. Xie B, Liu S, Wu S, et al. A novel bifunctional protein TNFR2-Fc-IL-1ra (TFI): expression, purification and its neutralization activity of inflammatory factors. *Mol Biotechnol.* 2013;54:141–147.
24. Tesic M, Sheldon KM, Ballinger JR, Boxen I. Labelling small quantities of monoclonal antibodies and their F(ab')2 fragments with technetium-99m. *Nucl Med Biol.* 1995;22:451–457.
25. Mishra AK, Iznaga-Escobar N, Figueredo R, et al. Preparation and comparative evaluation of ^{99m}Tc-labeled 2-iminothiolane modified antibodies and CITC-DTPA immunoconjugates of anti-EGF-receptor antibodies. *Methods Find Exp Clin Pharmacol.* 2002;24:653–660.
26. Min JY, Chen Y, Malek S, et al. Stem cell therapy in the aging hearts of Fisher 344 rats: synergistic effects on myogenesis and angiogenesis. *J Thorac Cardiovasc Surg.* 2005;130:547–553.
27. Nikolaidis LA, Doverspike A, Huerbin R, Hentosz T, Shannon RP. Angiotensin-converting enzyme inhibitors improve coronary flow reserve in dilated cardiomyopathy by a bradykinin-mediated, nitric oxide-dependent mechanism. *Circulation.* 2002;105:2785–2790.
28. *Guide for the Care and Use of Laboratory Animals*. Bethesda, MD: National Institutes of Health; 1985. NIH publication 85-23.
29. van Eerd JE, Oyen WJ, Harris TD, et al. Scintigraphic imaging of infectious foci with an ^{111}In-LTB4 antagonist is based on in vivo labeling of granulocytes. *J Nucl Med.* 2005;46:786–793.
30. van Eerd JE, Broekema M, Harris TD, et al. Imaging of infection and inflammation with an improved ^{99m}Tc-labeled LTB4 antagonist. *J Nucl Med.* 2005;46:1546–1551.
31. Lee WW, Marinelli B, van der Laan AM, et al. PET/MRI of inflammation in myocardial infarction. *J Am Coll Cardiol.* 2012;59:153–163.
32. Cawthorne C, Prenant C, Smigova A, et al. Biodistribution, pharmacokinetics and metabolism of interleukin-1 receptor antagonist (IL-1RA) using [^{18}F]-IL1RA and PET imaging in rats. *Br J Pharmacol.* 2011;162:659–672.
33. van der Laken CJ, Boerman OC, Oyen WJ, van de Ven MT, van der Meer JW, Corstens FH. Imaging of infection in rabbits with radioiodinated interleukin-1 (alpha and beta), its receptor antagonist and a chemotactic peptide: a comparative study. *Eur J Nucl Med.* 1998;25:347–352.
34. Ono K, Matsumori A, Shioi T, Furukawa Y, Sasayama S. Cytokine gene expression after myocardial infarction in rat hearts: possible implication in left ventricular remodeling. *Circulation.* 1998;98:149–156.
35. Yue P, Massie BM, Simpson PC, Long CS. Cytokine expression increases in nonmyocytes from rats with postinfarction heart failure. *Am J Physiol.* 1998;275: H250–H258.
36. Grünenfelder J, Miniati DN, Murata S, et al. Upregulation of Bcl-2 through caspase-3 inhibition ameliorates ischemia/reperfusion injury in rat cardiac allografts. *Circulation.* 2001;104:I202–I206.
37. Berthonneche C, Sulpice T, Boucher F, et al. New insights into the pathological role of TNF-alpha in early cardiac dysfunction and subsequent heart failure after infarction in rats. *Am J Physiol Heart Circ Physiol.* 2004;287:H340–H350.
38. Toufektsian MC, Robbez-Masson V, Sanou D, et al. A single intravenous sTNFR-Fc administration at the time of reperfusion limits infarct size–implications in reperfusion strategies in man. *Cardiovasc Drugs Ther.* 2008;22:437–442.
39. Wallach D, Engelmann H, Nophar Y, et al. Soluble and cell surface receptors for tumor necrosis factor. *Agents Actions Suppl.* 1991;35:51–57.
40. Kriegler M, Perez C, DeFay K, Albert I, Lu SD. A novel form of TNF/cachectin is a cell surface cytotoxic transmembrane protein: ramifications for the complex physiology of TNF. *Cell.* 1988;53:45–53.